DISTINGUISHING SIGNAL CONTRIBUTIONS FROM BULK FLUID AND CHANNEL SURFACE REGIONS TO IMPROVE BACKSCATTERING INTERFEROMETRY SIGNAL

By

Joseph McConkie Evans

Thesis

Submitted to the Faculty of the

Graduate School of Vanderbilt University

in partial fulfillment of the requirements

for the degree of

MASTER OF SCIENCE

in

Biomedical Engineering

May, 2014

Nashville, Tennessee

Approved:

Darryl J. Bornhop, Ph.D.

Frederick R. Haselton, Ph.D.

ACKNOWLEDGMENTS

I would like to thank my advisor, Dr. Rick Haselton, as well as Dr. Darryl Bornhop for their guidance and support. Also, this research would not have been possible without help from members of the Bornhop lab, especially Amanda Kussrow, Michael Kammer, Dan Dugmore, and Phoonthawee Saetear. Finally, I want to acknowledge my wife and son, Shelby and Sam. Their love and support was invaluable to me. They provided me with the motivation to complete this work.

Table of Contents

Page

LIST OF TABLES

Table Page

LIST OF FIGURES

Figure Page

Chapter I

INTRODUCTION

Noninvasive, highly sensitive, and accurate diagnostic tests are needed to reduce deaths from diseases such as lung cancer[4]. One of the challenges of doing tests based on the presence of specific biomarkers is that where current tests do not detect biomarkers in low enough concentrations at early stages of the disease. As additional biomarkers are identified there will be an increasing need for this type of test for infectious, cardiovascular, pulmonary, and metabolic diseases as well. Interaction assays are employed in many sensing applications [2, 5]. For example, they are used to quantify the presence of a target, such as a disease biomarker or pollutant, to determine mechanism of action for ligand receptor binding [6-8] or to estimate first in-human dosing for new drugs [9-11]. There are many methods that have been used to determine if a pair of reactants have interacted or to measure the affinity for a biomolecular binding event, including UV-vis, fluorescence, NMR and mass spectrometry (MS). The central nature of interaction determinations and desire to perform chemical and biochemical measurements with high accuracy has spawned the development and refinement of label-free technologies. These include plasmonic sensors such as surface plasmon resonance (SPR)[5], interferometric devices such as the bio-layer interferometer [2, 12], and hybrid systems like interferometric SPR [13, 14]. While useful, all of these approaches require surface immobilization of one of the interacting species and cannot be used to perform studies in free-solution.

Surface Plasmon Resonance

SPR sensors are well-known label-free biosensors. The fundamental phenomenon of SPR is the oscillation of electrons in a solid or liquid that occurs in reaction to light stimulation. The refractive index

(RI) of a transducing medium changes in response to the quantity of the molecule of interest. This change in RI can be determined by interrogating the SPR [15]. Commercialized SPR sensors typically have a prism that couples the light to the transducing medium and have detection limits between 1 X 10^{-6} and 1 X 10^{-7} [16]. A schematic of a typical SPR sensor configuration is shown in Figure 1 [1]. While these detection limits are good for research purposes, they cannot differentiate between bulk and surface RI changes. Also, they can only penetrate about 100 nm into the medium [16], making it difficult to detect large targets such as cells and bacteria. There are other very sensitive SPR biosensors, such as long range surface plasmon and short range surface plasmon, that can differentiate between bulk RI changes and surface RI changes [17] but they can only detect one type of analyte [16]. SPR is not used to detect analytes in free solution, but rather in a tethered format. SPR is used to determine a number of interaction phenomena, such as whether two molecules interact directly and the interactions kinetic and thermodynamic properties. It can also be used to detect the presence and concentration of a molecule in a solution, such as a biomarker for a specific disease, as well as protein surface adhesion to metal surfaces and nanoparticles.

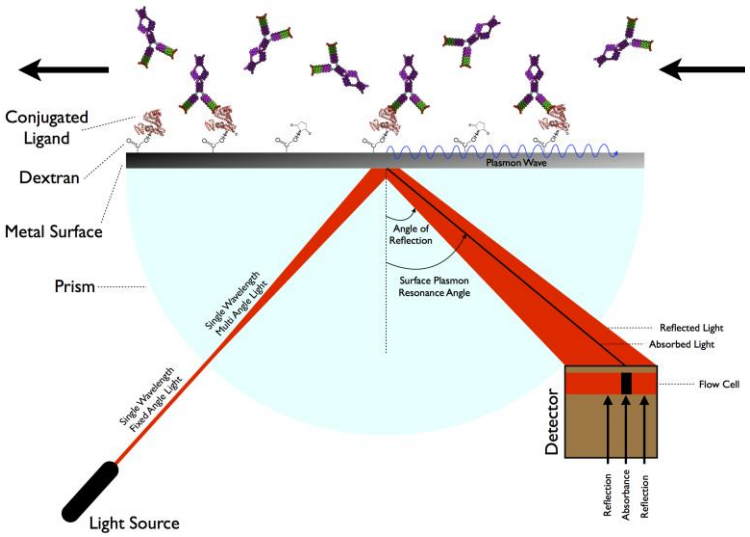

Figure 1- Schematic of Surface Plasmon Resonance (SPR) configuration [1]. A single wavelength of light is guided to a metal surface where a tethered dextran resides to bind to the analyte of interest. Light excites electrons when it makes contact with the metal, causing a plasmon wave. Analyzing reflected and absorbed light using a detector can give insight into the binding taking place on the surface.

Acoustic and Calorimetric Sensors

Other biosensors can detect molecules without labels as well, such as acoustic and calorimetric sensors. They do so by monitoring changes in resonant frequencies of quartz crystal resonators [18]. A

linear relationship between the mass adsorbed to the surface of the crystal and its resonant frequency was discovered by Sauerbrey in 1959. These types of sensors have a mass sensitivity of 3 X 10^{-2} g mm^{-2} [18]. Because the mass of the molecule of interest has to be in direct contact with the crystal this method cannot be used in a free solution format. Calorimetric sensors measure the heat generated when substances bind to each other, for example enzyme catalyzed reactions such as a series of statins to HMG-CoA reductase [19]. These reactions are exothermic and produce heat that can be used to measure the rate of the reaction, and this rate can be used to measure analyte concentrations. Binding constants can be determined by measuring the enthalpy and entropy resulting from the interaction [19]. Calorimetry methods have been limited in their application because they require large amounts (>µmol/L) of the receptor and ligand [18], limiting throughput.

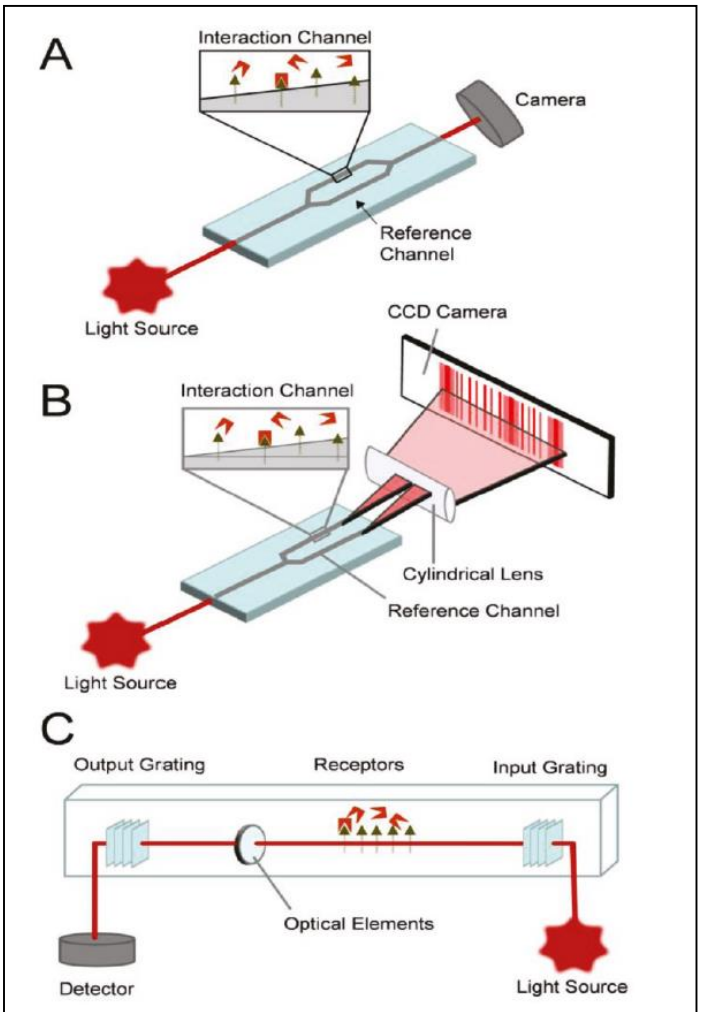

Figure 2- Schematic of A) Mach-Zehnder interferometer (MZI), B) Young interferometer (YI), C) Hartman interferometer (HI) [2]. In all three configurations, incoming light interacts in regions where analytes of interest bind and resultant phase shifts of the outgoing are measured.

Mach-Zehnder Interferometer

Another class of label free biosensors use interferometry, where multiple light waves interact to create interference patterns. This interference pattern depends, in part, on the mediums through which the light has traveled. Changes in the medium produce changes in the interference pattern of the light that can be studied to gain insights into the

medium, such as molecular binding events that cause RI changes. Three interferometers are shown in Figure 2 [2], which I discuss here. The Mach-Zehnder interferometer (MZI) measures binding induced changes in RI within an evanescent field. MZI uses a waveguide to monitor differences in RI between a sample and reference [2]. Recombining the two beams, which interfere with each other after going through different mediums, produces a phase shift in the sensor arm beam, which in turn changes the output intensity of the beam. One of the strengths of MZI is that it nearly eliminates temperature induced shifts in RI [20], but it is difficult to measure low concentrations of analyte without using large sample volumes [21]. Early configurations of MZI resulted in detection limits of 2×10^{-2} refractive index units (RIU) [22] but a more recent total internal reflection configuration of MZI was developed that reached a detection limit of 7×10^{-6} RIU while sensing the interaction between an immobilized pesticide and its antibody in phosphate buffered saline Tween (PBST) [23]. Initial biosensing demonstrations detected fetal calf serum non-specifically binding to the sensor surface [22].

Young Interferometer

The Young interferometer (YI) is similar to MZI in that there are two waveguides to guide beams through a sample and a reference. YI does not recombine the beams into one, as MZI does, but lets them interact in free space. The resulting interference pattern is captured by a CCD camera [2]. Waveguide channels can be multiplexed within this interferometer and has been shown to measure RI changes as small as 8.5×10^{-8} RIU [24]. YI has been used to detect 21-mer DNA with receptor DNA immobilized on the surface of the sensor with a refractive index detection limit of 0.9×10^{-6} [25].

Hartman Interferometer

Another interferometer, known as the Hartman interferometer (HI), also uses waveguides. Planar waveguides are employed that have rows patterned in them to immobilize molecules. A grating produces a broad beam that enters the waveguide, interacts with the different species immobilized in the different lines of the waveguide, and recombines to produce interference [2]. Again, the phase shift of this interference pattern in measured to make determinations regarding the species being

interrogated. HI has been shown to overcome problems associated with non-specific binding that occurs in complex biological samples, such as serum, by using a reference region and controlled surface chemistry [26].

Dual Polarization Interferometer

Dual Polarization interferometers (DPI) also use two waveguides, for a sample and reference, which are stacked on top of each other so they can be illuminated by a single laser beam. The polarization of the laser used in DPI is alternated between two modes in order to modulate the signal and increase its sensitivity [2]. Measuring the polarization and RI of the light coming out gives information regarding the thickness of an adsorbed protein layer [2]. DPI has been shown to measure interactions for a large range of analyte sizes, as well as measuring kinetics and structure at the same time [27, 28]. For example, this was done with D-biotin interacting with streptavidin [3]. The sensitivity of the interferometers mentioned so far, as well as others, is enhanced with longer optical path lengths in contact with the analyte of interest. The more the light interacts with the analyte, the greater the phase shift of the outgoing light, and the greater the signal produced. As a result, the instrumentation involved in building these sensors are usually measured on the order of centimeters.

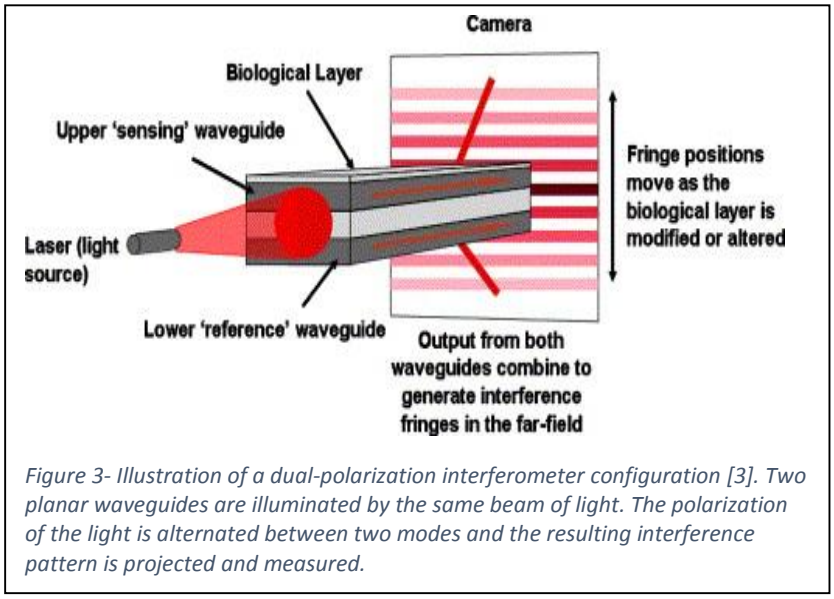

Figure 3- Illustration of a dual-polarization interferometer configuration [3]. Two planar waveguides are illuminated by the same beam of light. The polarization of the light is alternated between two modes and the resulting interference pattern is projected and measured.

Waveguide Microresonators

Waveguide microresonators can measure interactions, label free, with high sensitivity. They do so by taking advantage of multiple passes of light encountering an analyte, rather than just one pass like those that use waveguides. This is due total reflectance being employed in a circular configuration,

which enhances the Q (resonance) factor of the instrument. Small molecules binding to the resonator change the RI on the surface and disrupts the resonance wavelength. Recirculation of the light inside the resonator results in a narrower resonance line width [2]. This narrower resonance line width results in a higher Q factor, which has been shown to be related to greater sensitivity [29]. Difficulty dealing with alignment issues lead to the development of multiplexing this method using lithography and simple optical communication technologies [30, 31]. On-chip micro-ring resonators used in an array format have been able to detect protein cancer biomarkers in pure serum sensitively enough to be relevant clinically [30]. This technology has great potential because of its high sensitivity and multiplexing capabilities.

Porous Sensors

Another class of sensors utilizes pores etched into materials such as silicon, titanium, and aluminum. These porous thin films act as an interferometer by creating an interference pattern from light reflecting off different surfaces within the sensor, in this case the top and bottom portions of the pores. Pore size can be varied depending on what the analyte of interest is, but generally smaller pores result in greater sensitivity [32]. In biomolecular interaction applications specifically, functionalized portions and their bound substrates reside inside the pores, causing light to interact differently on these surfaces [2]. Because the principle by which these types of sensors work is based on reflective interferometry, they measure optical density, which is a function of RI and layer thickness. One advantage of this is that the temperature does not need to be controlled as precisely as it does in other methods. This is because RI and layer thickness

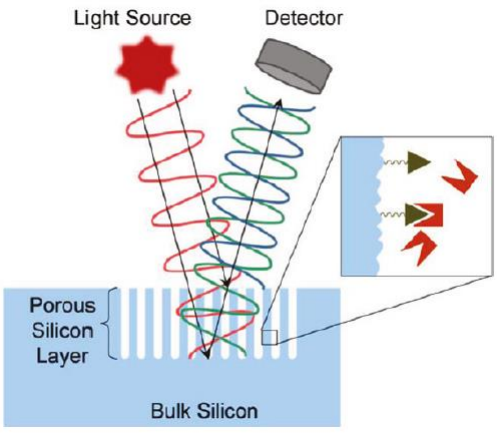

Figure 4- Porous sensor schematic [2]. The interference pattern in porous sensors results from light interacting with analytes binding to the surface inside the pores.

essentially compensate for each other as temperature changes. For example, when temperature rises, the layer thickness increases due to thermal expansion, while the RI decreases, and visa-versa[33, 34]. Porous sensors have been shown to detect the binding of DNA oligomers, proteins, and other small molecules in pico- and femtomolar concentrations [35].

Backscattering Interferometry

A relatively new interferometric methodology, backscattering interferometry (BSI), has a significant advantage over these other sensing methods because it can be used in either label-free format, tethered or free-solution [36-39]. There are advantages to both formats, with tethered assays being particularly valuable when there is a need to deploy the test to a remote location or in a near patient setting. Free-solution determinations, without labels, provide an unperturbed environment for determining if a ligand and receptor bind and give the most accurate measure of affinity. In addition, free-solution assays are rapid, less complex, cost less, and don't risk the potential of biasing or perturbing the outcome [18, 40].

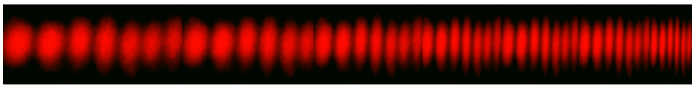

Figure 5- Composite photograph of 47 interference fringes produced by backscattering interference of light from a laser impinging on a fluid filled microchannel onto a 1 inch CCD array camera. For more detail please refer to Figure 6.

Unlike any other method, BSI is a unique interferometer, impinging coherent parallel rays from a laser onto a fluid-filled microchannel. While other instrument components are measured in the order of centimeters, as mentioned above, the channel in which light interacts in the BSI instrument is on the order of only 10s of micrometers. As described previously [8], the light-chip interaction leads to a fan of scattered light containing a high contrast interference fringe pattern (Figure 5). Measuring the spatial shift in the fringes has enabled the detection of numerous types and classes of biomolecular interactions [38, 39, 41, 42], with high sensitivity and in complex matrices [43].

Biomolecular binding events can be measured by BSI because changes in the refractive index (RI) of the medium which is principally a consequence of changes in conformation, hydration and electrostatics [44, 45], can be detected by measuring the spatial shifts of the fringes. Because of this, BSI is minimally affected by the relative mass of the two interactants, which is not the case for sensing methods such as SPR. Correlation of these fringe shifts with analyte concentration in the fluid provides high sensitivity (picomolar K_d and detection limits on the order of thousands of molecules), label free quantification of a vast array of molecules such as protein-protein interactions, ion-protein interactions, small molecule-protein interactions, membrane-ligand interactions, carbohydrate-lectin binding, and aptamer-protein interactions[38, 39, 41, 42].

Protein adsorption to glass is a well-known phenomenon [46-48] and proteins that adhere to the glass channel surface undergo conformational changes[46]. This is a problem when detecting interactions in free solution using BSI because light interacting on the surface of the channel is affected by surface composition. Changes on the surface due to protein adsorption contribute unwanted noise to the signal. One approach to eliminate contributions from surface binding is to reduce protein adhesion at liquid-glass interfaces. These methods require physical modification of either the glass surface or the proteins involved in the interaction, but some protein adhesion inevitably still occurs [49] and manipulation of the surface of the channel affects the signal produced by BSI[38, 41, 50, 51]. While this is not a problem in a tethered format used by the instruments covered above, it can be problematic when the analyte of interest is in free solution, as it is in BSI. SPR, which uses a tethered format, automatically distinguishes the surface from the bulk binding signal because the evanescent wave couples only about one hundred nanometers into the solution [52], but since BSI can work in both configurations and the optical interrogation method inherently combines the surface and the bulk signal, there is a desire to optimize performance under the most appropriate assay configuration.

Although we have shown that BSI can be used to make interaction measurements at efficacious performance levels, even in complex matrices[38, 43], improvements in S/N are desirable and could simplify the use of the technique. Non-specific protein adsorption has, and continues to be, a major limitation in the application of biosensors such as SPR [53]. Many approaches have been employed to reduce or eliminate surface fouling, most of them involving some form of surface pacification chemistry [54]. BSI is not immune to this phenomenon, with adsorption to the surface of the channel producing a signal as a result of changes in the optical path of the interferometer. Because the BSI signal is an ensemble measurement resulting from the refraction of light at all interfaces, under conditions where the amount of material adhered to the surface changes throughout the assay or from run-to-run on replicate determinations, the contribution of the signal from the changing surface can lead to a reduction in the reproducibility of the measurement and negatively affect the limit of quantification (LOQ)[43].

Previous signal analysis methods used in BSI [55] include taking the cross-sectional intensity profile of a small, contiguous subset of the fringes and performing a fast-Fourier transform (FFT) on them. This is done using 4-8 of the fringes in a region of the fringe pattern that exhibits a single spatial frequency. The specific fringes analyzed vary between different experiments but typically reside in the first half of the fringe pattern, beginning from the left. The phase of the dominant frequency, which is a measure of the spatial shift, is then monitored [5]. This analysis method ignores signal content contained in the other fringe subsets and less dominant frequencies. Since BSI can measure *either* surface immobilized or free-solution binding events, we hypothesize that one region in the fringe pattern could be signaling binding events on the surface and another region could be signaling binding events in the bulk solution [51].

Here we report an approach to reducing the impact of non-specific surface binding on the BSI signal by using a fringe pattern interrogation method to identify differences in the fringe pattern for the

signal produced at the surface or the bulk. We have found that the signal produced by BSI, in a response to a change in the RI of the bulk fluid, can be discriminated from a change in RI produced when molecules bind to the surface. Using two model assay systems, producing known bulk and surface RI changes, we developed an algorithm to identify signal changes in response to bulk RI while eliminating the contribution of the signal produced by surface bound species. The algorithm can automatically find these fringe features and allow the user to display the experimental result as a composite, bulk, or surface binding signal.

Chapter II

DISTINGUISHING SIGNAL CONTRIBUTIONS FROM BULK FLUID AND CHANNEL SURFACE REGIONS IN BACKSCATTERING INTERFEROMETRY

Abstract

Backscattering Interferometry (BSI) has been used to detect bio-molecular interactions by measuring shifts in the bulk refractive index of a sample due to conformational changes occurring upon binding. BSI has advantages over other biosensors because of its sensitivity and it can detect interactions in free solution, as well as in a tethered format. Previous studies have demonstrated interaction assays with BSI in a surface tethered configuration and demonstrated the free-solution determinations using the same fringes and analysis algorithm. So when performing an assay in free-solution the signal detected must be an ensemble measurement of both the surface and bulk signal. In the past, proper controls, rinsing procedures and channel wall coatings has enabled discrimination of the non-specific surface adsorption from the signal of interest generated in the bulk. Even so, these unwanted surface-derived signals reduce the reproducibility of BSI assays and negatively affecting its limit of quantification. Here I show that there are regions within the spatial and frequency domains of the fringe pattern that are sensitive only changes in the bulk fluid. This observation allowed the development of a procedure and algorithm to be developed that enables rejection of the surface signal with minimal impact on the signal to noise ratio for the bulk signal. Two model systems were designed in which the surface conditions of the glass microchannel, as well as the bulk fluid, were changed in a controlled manner. Step changes in glycerol concentration in the bulk fluid were made and successive layers were chemically coupled to the surface to produce independent bulk and surface signals. Non dominant frequencies, as well as all contiguous fringe subsets of the fringe pattern, previously uninvestigated, allowed distinct regions to be identified that are sensitive to bulk RI, but that are

insensitive to the surface changes. The algorithm tabulates the phase output of each frequency, within each contiguous fringe subset, and outputs those subsets that show no signal from surface changes, but maintains signal produced by bulk fluid changes. Thus by analyzing these regions of interest specifically, unwanted signal contributions from surface adhesion are effectively eliminated while the signal produced by the bulk fluid is maintained. Multiple regions in each data set, within each model, were found that are insensitive to surface binding. One limitation of the method is a reduction in signal to noise ratio performance when the algorithm is applied to give a discrete output. The signal to noise ratio using the previous analysis method was 3.56, while using the new algorithm resulted in a signal to noise ratio of 2.98. By summing frequencies and regions of interest, the signal to noise ratio of this new analysis can be increased by as much as 59%.

Introduction

Noninvasive, highly sensitive, and accurate diagnostic tests are needed to reduce deaths from diseases such as lung cancer[4]. One of the challenges of doing tests based on the presence of specific biomarkers is that where current tests do not detect biomarkers in low enough concentrations at early stages of the disease. As additional biomarkers are identified there will be an increasing need for this type of test for infectious, cardiovascular, pulmonary, and metabolic diseases as well. Interaction assays are employed in many sensing applications [2, 5]. For example, they are used to quantify the presence of a target, such as a disease biomarker or pollutant, to determine mechanism of action for ligand receptor binding [6-8] or to estimate first in-human dosing for new drugs [9-11]. There are many methods that have been used to determine if a pair of reactants have interacted or to measure the affinity for a biomolecular binding event, including UV-vis, fluorescence, NMR and mass spectrometry (MS). The central nature of interaction determinations and desire to perform chemical and biochemical measurements with high accuracy has spawned the development and refinement of label-free technologies. These include plasmonic sensors such as surface plasmon resonance (SPR)[5], interferometric devices such as the bio-layer interferometer [2, 12], and hybrid systems like interferometric SPR [13, 14]. While useful, all of these approaches require surface immobilization of one of the interacting species and cannot be used to perform studies in free-solution.

Previous signal analysis methods used in BSI [55] include taking the cross-sectional intensity profile of a small, contiguous subset of the fringes and performing a fast-Fourier transform (FFT) on them. This is done using 4-8 of the fringes in a region of the fringe pattern that exhibits a single spatial frequency. The specific fringes analyzed vary between different experiments but typically reside in the first half of the fringe pattern, beginning from the left. The phase of the dominant frequency, which is a measure of the spatial shift, is then monitored [5]. This analysis method ignores signal content contained in the other fringe subsets and less dominant frequencies. Since BSI can measure *either*

surface immobilized or free-solution binding events, we hypothesize that one region in the fringe pattern could be signaling binding events on the surface and another region could be signaling binding events in the bulk solution [51].

Here we report an approach to reducing the impact of non-specific surface binding on the BSI signal by using a fringe pattern interrogation method to identify differences in the fringe pattern for the signal produced at the surface or the bulk. We have found that the signal produced by BSI, in a response to a change in the RI of the bulk fluid, can be discriminated from a change in RI produced when molecules bind to the surface. Using two model assay systems, producing known bulk and surface RI changes, we developed an algorithm to identify signal changes in response to bulk RI while eliminating the contribution of the signal produced by surface bound species. The algorithm can automatically find these fringe features and allow the user to display the experimental result as a composite, bulk, or surface binding signal.

Methods

The BSI instrument configuration utilized in this study is shown in Figure 6 and has previously been described in detail [56]. Typically BSI signals are a transduced by capturing 4-8 fringes and measuring their spatial shifts using the frequency with the highest power in the Fourier domain of the fringe subset [5]. In the experiments performed in this study, the camera, initially positioned at a distance of 45 cm from the mirror, was moved to 3.5 cm away. This dimension is labeled “d” in Figure 6.

This allowed us to capture more than 60 fringes for analysis. In order to develop an algorithm that automatically distinguishing between signal originating from surface changes and signal originating from the bulk fluid region of the channel, we developed two models. In both model systems, a variety of bulk fluid content and surface bound molecules were applied in the channel in succession. By controlling the surface layers and bulk fluid content we were able to produce signal originating from known changes in the surface and bulk regions independently. An algorithm was then developed to analyze these independent signals to find regions within the fringe pattern that *only* responded to changes in the bulk fluid content, regardless of surface contamination.

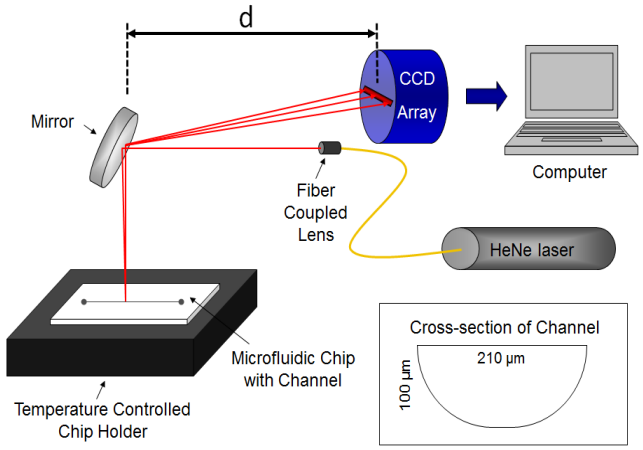

Figure 6- BSI instrument schematic. A He-Ne laser is directed from a fiber coupler to the microfluidic channel via a mirror. The backscattered light is then directed, via the same mirror, onto a CCD array camera and recorded in LabVIEW.

In the first model system, 4 concentrations of glycerol in phosphate-buffered-saline (PBS) were used to produce changes in bulk refractive index with no surface layer bound to the channel surface. Glycerol was chosen because it produces a linear shift in the refractive index of the bulk fluid. The specific glycerol concentrations (0 mM, 2 mM, 6 mM, and 10 mM) were chosen because they are easy to produce accurately using simple dilution methods. A surface layer was then added to the channel using 3-mercaptopropyltriethoxysilane (MEPTES) to mimic surface binding. Four measurement were taken with 0mM glycerol in PBS, followed by 4 more glycerol concentration changes in PBS. Each of the twelve samples and their associated bulk and surface content is outlined in Table 1.

A CCD camera was used to record 50 frames of the fringe pattern produced by each sample described in Table 1. Data was taken for samples 1-4 before the addition of MEPTES to the surface of the channel. Next, the surface of the channel was cleaned by soaking the channel in 10% KOH in methanol for 30 minutes. Then the channel was rinsed with deionized water and dried with dry compressed air. The channel was then rinsed with Toluene. Next, the channel was soaked in 2% 3-mercaptopropyltriethoxysilane (MEPTES) in toluene for 60 min in order to silanize the glass surface. The channel was again rinsed using Toluene. After rinsing with deionized water and drying, samples 5-12, along with associated bulk fluid content shown in Table 1, were analyzed. An illustration of the silanization process is shown in Figure 7.

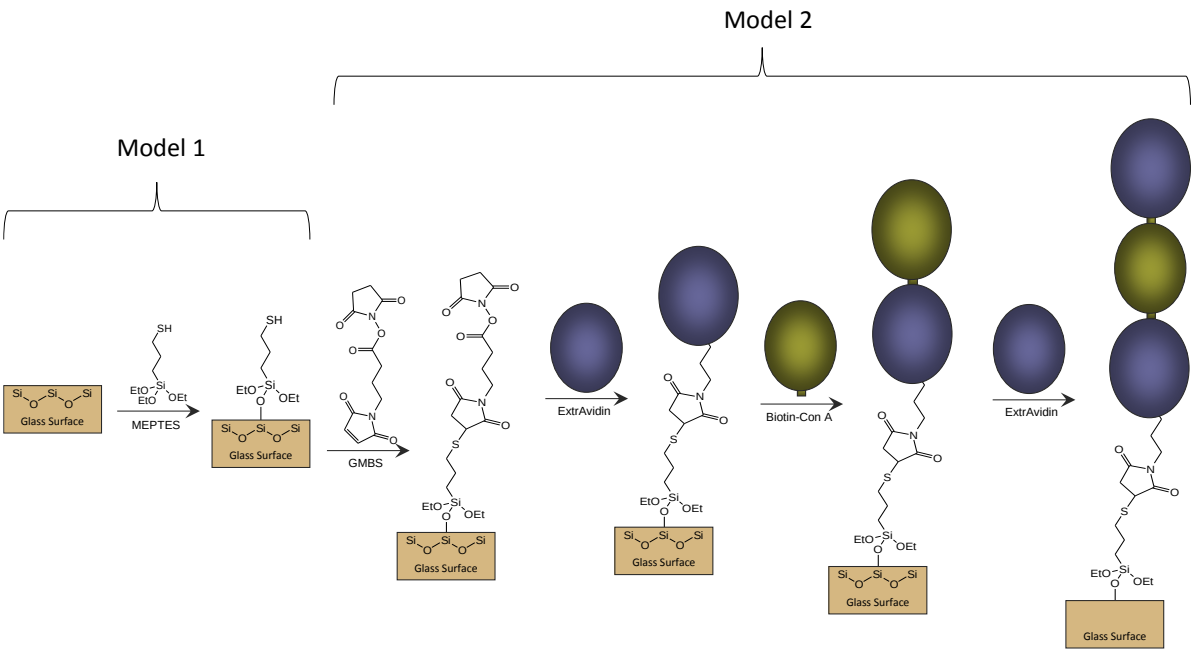

Figure 7- Steps of microchannel surface layer preparation. For model 1, MEPTES is applied to silanize the surface of the glass. For model 2, a layer of GMBS is added, followed by ExtrAvidin, Biotin-BSA, and then a second layer of ExtrAvidin.

Bulk Content	**0mM** Glycerol in PBS	**2mM** Glycerol in PBS	**6mM** Glycerol in PBS	**10mM** Glycerol in PBS	**0mM** Glycerol in PBS	**0mM** Glycerol in PBS	**0mM** Glycerol in PBS	**0mM** Glycerol in PBS	**0mM** Glycerol in PBS	**2mM** Glycerol in PBS	**6mM** Glycerol in PBS	**10mM** Glycerol in PBS
Surface Layers					MEPTES	MEPTES	MEPTES	MEPTES	MEPTES	MEPTES	MEPTES	MEPTES
	S1	**S2**	**S3**	**S4**	**S5**	**S6**	**S7**	**S8**	**S9**	**S10**	**S11**	**S12**

Table 1 – Model 1: Each data set consisted of BSI signals obtained under 12 different sample conditions (S1-S12). This table lists the bulk fluid content of the microchannel and the surface bound molecule layers present for each of the 12 samples in model 1.

In the second model system the bulk fluid content was changed to water and 4 more surface layers were applied to produce the surface signal. Different bulk content and surface layers between model 1 and model 2 were chosen to make sure that our analysis method can be extended to more than one system. First, a 4-step glycerol in water concentration gradient was produced. N-(γ-maleimidobutyryloxy)succinimide ester (GMBS) was added as the first surface layer, followed by ExtrAvidin, BSA-Biotin, then another layer of ExtrAvidin. An illustration of this process is shown in Figure

Bulk Content	**0mM** Glycerol in Water	**2mM** Glycerol in Water	**6mM** Glycerol in Water	**10mM** Glycerol in Water	**0mM** Glycerol in Water	**0mM** Glycerol in Water	**0mM** Glycerol in Water	**0mM** Glycerol in Water	**0mM** Glycerol in Water	**2mM** Glycerol in Water	**6mM** Glycerol in Water	**10mM** Glycerol in Water
Surface Layers								ExtrAvidin	ExtrAvidin	ExtrAvidin	ExtrAvidin	ExtrAvidin
							BSA-Biotin	BSA-Biotin	BSA-Biotin	BSA-Biotin	BSA-Biotin	BSA-Biotin
						ExtrAvidin	ExtrAvidin	ExtrAvidin	ExtrAvidin	ExtrAvidin	ExtrAvidin	ExtrAvidin
					GMBS	GMBS	GMBS	GMBS	GMBS	GMBS	GMBS	GMBS
	S1	**S2**	**S3**	**S4**	**S5**	**S6**	**S7**	**S8**	**S9**	**S10**	**S11**	**S12**

Table 2- Model 2: Each data set consisted of BSI signals obtained under 12 different conditions. This table lists the bulk fluid content of the microchannel and the surface bound molecule layers present for each of the 12 samples (S1-S12) in model 2.

7. Table 2 shows the 12 samples and their surface and bulk content.

50 frames of each sample we recorded in the same manner as model 1. Samples 1-4, along with associated bulk fluid content shown in Table 2, were analyzed. After the channel was rinsed and dried, the silanized chip was then soaked in 1 mM N-(γ-maleimidobutyryloxy)succinimide ester (GMBS) in absolute ethanol for 30 min. Once again, the channel was rinsed with deionized water and dried and sample 5 was analyzed. The channel was then rinsed and dried before soaking in an ExtrAvidin solution (1 mg/mL) for 2 ½ hours. Sample 6 was then analyzed. Having coated the channel with ExtrAvidin any biotinylated molecule of interest can be immobilized onto the surface by soaking for 60 minutes. BSA-Biotin was then added as an additional layer in like manner for sample 7. Sample 8 consisted of an additional layer of ExtrAvidin. Each of the samples 5-8 were analyzed with deionized water residing in the channel. An illustration of this process is shown in Figure 7. More detail regarding layer thickness and surface characterization was reported previously (Olmstead, et al) [56]. Data from samples 9-12 were collected the same manner as samples 1-4 but with the surface chemistry present.

Each sample (S1 to S12, illustrated in Tables 1 and 2) produces a fringe pattern. The fringe pattern was then modeled by measuring the cross-sectional intensity of the fringes, as shown in Figure 8-c. An FFT was performed on each contiguous fringe subset to determine its frequency content. Since in this approach the important regions of the fringe pattern are unknown, we simply evaluated every possible contiguous subset. In total, 9×10^5 different parameter combinations are analyzed by the program. Each frequency in this frequency domain (Figure 8-d) has an associated phase. The magnitude of each phase, calculated at a single frequency within a subset of fringes, was measured in radians. This magnitude, relative to the baseline sample, constitutes the signal and was recorded as the output from the analysis. A program was written in LabVIEW to analyze 50 frames of each sample (1-12) and the associated position of all available fringes (see Figure 8-c).

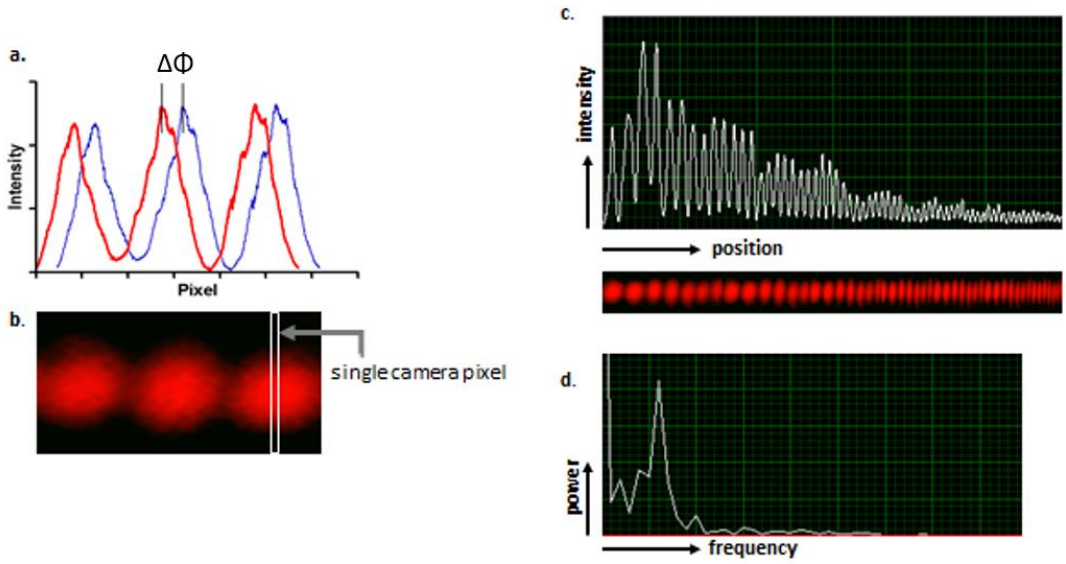

Figure 8- a) Intensity profile of 3 fringes of two different samples at different phases. The spatial shift of the fringes from red to blue are plotted in the inlayed phase plot with phase differences corresponding to the red and blue lines. b) Backscattered fringes as seen with the naked eye aligned below the intensity profile to show the intensity relationship (aligned with the intensity profile above it shown in 4-a). The CCD camera is a 1-dimensionally arrayed camera with vertically stretched pixels as shown. Each value in the intensity profile in 4-a represents the average intensity of each pixel. c) Intensity profile of 60 fringes being captured by the camera. The red dots below the plot show the fringes as seen with the naked eye. d) Fourier output of 4-c.

The algorithm, referred to as the surface vs. bulk (SvB) algorithm, analyzes each frequency of the discrete Fourier transform (frequency domain) of each contiguous subset of fringes within the total set of fringes captured by the camera. All possible contiguous subsets of fringes are analyzed. Contiguous subsets were analyzed in this study for two reasons. First, this was the strategy used to analyze BSI data in previous experiments [1, 5]. Second, it is computationally simple to do so. Other methods could have been attempted, such as analyzing all possible non-contiguous fringe subsets, but this would drastically increase the complexity of the algorithm. Contiguous subsets were therefore a logical and simple starting point for this new analysis.

The program output the phase of each sample for each fringe-frequency subset exhibiting signal produced from the bulk fluid and not from the surface layers. Algorithm parameters regarding the signal quality criteria, such as signal to noise thresholds and linear fits to the glycerol concentration gradients,

can be set by the user. For a fringe-frequency subset to qualify as one that exhibits signal from the bulk region (samples 1-4) of the channel and not from the surface (samples 5-8), it must pass these criteria. These criteria, along with their associated formulas, are presented in appendix A. The phase output from samples producing a bulk signal (samples 1-4) must pass a bulk signal criterion and the phase output from samples eliminating the surface signal (samples 5-8) must pass a surface signal criterion. A second glycerol concentration change in the bulk fluid (samples 9-12) is also included and compared to the first (samples 1-4). The algorithm compares the baseline of these two sets to make sure the surface signal has been eliminated and the second glycerol curve is not affected by the four surface layers. An algorithm flowchart is given in appendix B.

The fringe-frequency subsets that meet the criteria for a bulk signal being present, with no surface signal, were tabulated. These parameter subsets accurately reflect phase changes as the bulk fluid is changed, but no phase changes due to surface layers being added. The program allows the user to view the resultant phase plot for each fringe-frequency subset and records the window and frequency information used in the analysis. This information includes which fringes within the total fringe pattern are the first and last fringes in the window of fringes being output and which frequency is used in the analysis, in units of cycles/window. The signal to noise ratio and the slope for each glycerol gradient signal is also recorded. Program and data files are located on the external hard-drive in Darryl Bornhop's lab under the file-path, *Joe Evans/Surface vs Bulk*.

Results/Discussion

The purpose of this study is to find regions within the BSI signal that are not affected by changes to the surface of the channel, but are still sensitive to changes in the bulk fluid, in an attempt to improve the S/N of assays that suffer from poor signal due to surface adhesion to the glass microchannel. Since both signals are present in the dominant frequency we commonly analyze, run-to-run changes on the channel surface from non-specific adsorption of 'sticky' samples, such as proteins in serum, can

decrease the limit of quantification for an assay. Our preliminary optical modeling efforts (data not shown) indicated that some of the signal emanating from the surface of the chip would reside in a fringe-frequency subset that is different from that of the bulk solution.

To test this hypothesis we interrogated a large portion of the BSI fringe pattern by moving the camera closer to the chip (Figure 6) and independently changing the bulk fluid RI and that of the surface. By adding surface layers, in both model 1 and 2, it is shown that our hypothesis was confirmed. We found that for each data set there are multiple fringe-frequency subsets within the total set of fringes produced by BSI that report only the bulk or the surface signal.

Figure 9 includes 4 plots (a-d) that illustrate the signals produced from each of the twelve samples described in Table 1 and Table 2. The BSI signal is the magnitude of the phase shift of a subset of fringes. This is calculated in radians and shown on the vertical axes of these 4 plots. As this figure illustrates, each sample varies in signal magnitude due to variations in the surface and bulk contents of the channel. The x-axes of these plots denote the 12 different samples, with 50 data points taken by the camera of each sample. Thus, each sample in these plots includes 50 data points, leading to a step-like appearance between one sample and the next. All 50 data points for each sample are shown, rather than a single average value for each sample, to qualitatively illustrate the noise associated with each signal. These data points were recorded by the camera after each sample was prepared with its surface and bulk content, as described previously.

Figure 9-a and b shows the output of an experiment where the same samples were used but the data was analyzed in different ways. Figure 9-a illustrates the output using the previous signal analysis method used in BSI [55], where we select 4-8 fringes, in this case between fringe number 10 and 16, and record the phase shift of the dominant frequency. Note the signal difference between sample 1 and sample 5, both of which have the same bulk content (0mM glycerol in water) but sample 5 has no

MEPTES applied to the surface and sample 1 does. The different phase magnitude between these samples shows the signal produced by silanizing the surface of the channel with MEPTES. As expected, the baseline for the second glycerol curve (sample 9) is the same as sample 8, rather than sample 1 (the beginning of the first glycerol curve) due to the change in surface chemistry.

Figure 9-b shows the SvB algorithm analysis on the same data set, using the same samples. The SvB algorithm analyzes all of the fringes, scanning for the dominant and sub-dominant frequencies. Thus, each frequency within each fringe subset, together referred to as a fringe-frequency subset, has an associated signal, some of which only show signal when the bulk fluid is changed and no signal when the surface is modified. Other fringe-frequency subsets that eliminate the surface signal were found in addition to the one illustrated in Figure 9-b, but this one serves as an example. In this case we utilized the SvB algorithm to look at fringes 1-28 at a frequency of 34 cycles/window. The algorithm identified this fringe-frequency subset as one that did not show signal due to changes on the channel surface. It can be seen that sample 1 and sample 5 have the same signal magnitude, even though sample 5 had MEPTES added to the surface and sample 1 did not (see Table 1). The baseline for the second glycerol curve, starting at sample 9, has the same signal magnitude as the first (sample 1) when analyzed at this fringe-frequency subset. There were 90 other distinct fringe frequency subsets which likewise eliminated surface contributions to the signal. Another feature to note in this SvB algorithm output for model 1 is that the slope of the second glycerol concentration gradient (samples 9-12) is different from the first (samples 1-4). This is not totally unexpected since adding layers to the surface changed the interferometer in such a way that a different signal output may result. Although, we see that when the bulk fluid was changed from PBS to water in model 2 there was no longer any difference.

Figure 9-c and d show the output from data collected using model 2 (see Table 2) utilizing the previous and SvB algorithm analysis methods, respectively. The first surface layer of GMBS (sample 5) shows a signal magnitude different from sample 1, where no surface was present. Each subsequent

surface layer added (sample 6-8) also produce distinct signals. As was the case in model 1, the second glycerol curve (sample 9) starts at the same magnitude as the last surface layer (sample 8). This is expected because they have the same bulk and surface configurations, as shown in Table 2. The previous analysis method was used to generate the signal resulting from the dominant frequency between fringes 7 and 14 as shown in Figure 9-c, while Figure 9-d shows analysis of fringes 1-14 at the non-dominant frequency of 10 cycles/window. The surface signal of all 4 surface layers has been eliminated, as shown by samples 5-8 in Figure 9-d. Also, the second glycerol concentration gradient samples maintain the same slope and signal magnitude as the first (samples 1-2). Again, the algorithm successfully found regions in the BSI fringe pattern that produced signal from the bulk fluid but not the channel surface. In this particular data set there were 76 other fringe-frequency subsets exhibiting bulk signal but no surface signal output by the algorithm.

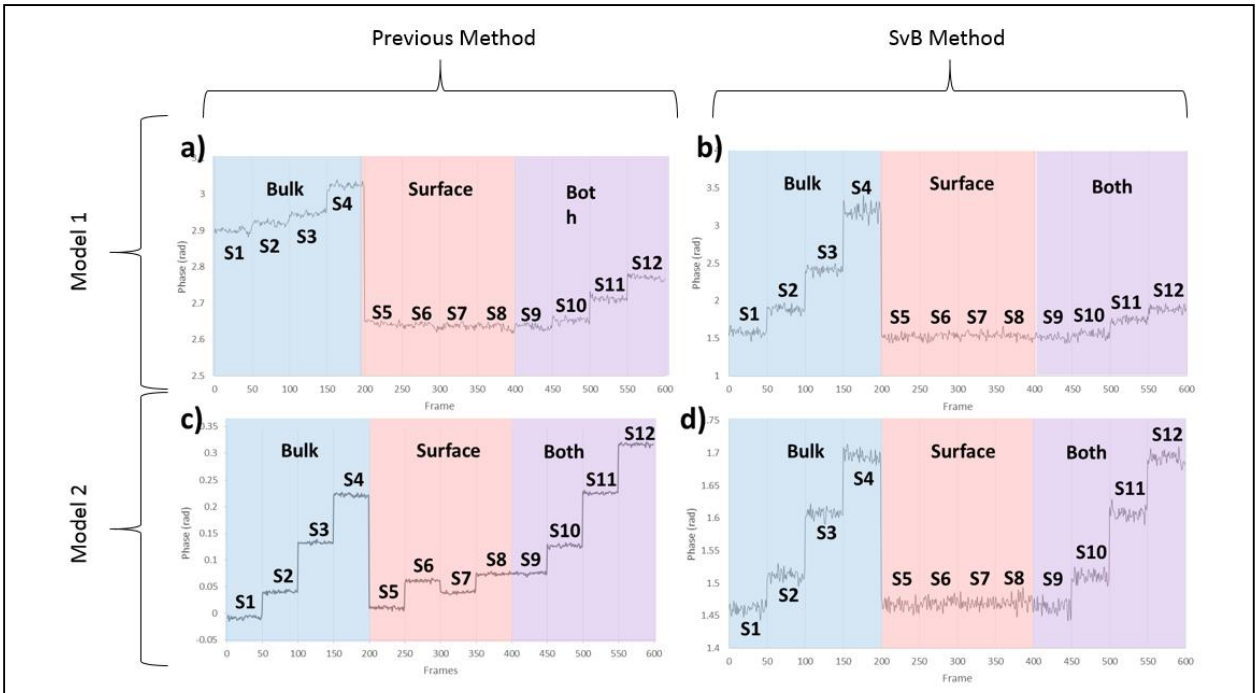

Figure 9- Basic output for a 12 sample data set as described in Tables 1 and 2 for model 1 and 2, respectively, showing signal from the bulk region (samples 1-4), surface (samples 5-8), and a combination of both (samples 9-12).The phase difference between samples (y-axis) denote the signal, while every 50 frames (x-axis) denote a unique sample, labeled S1, S2…S12. a) Fringe-frequency subset from model 1 where both bulk samples and surface sample produce a signal using the previous analysis method. b) Subset from model 1 that produces signal from the bulk samples but not the surface samples using the new analysis method. c) Fringe-frequency subset from model 2 where both bulk samples and surface sample produce a signal using the previous analysis method. b) Subset from model 2 that produces signal from the bulk samples but not the surface samples using the new analysis method.

Careful evaluation of the previous analysis method in Figure 9-c, versus the new analysis method in Figure 9-d, shows that there is a deterioration in S/N from the previous method to the SvB method. This is the same for plots shown in Figure 9-a and b, respectively. This is likely due to the fact that the frequency at which the surface signal disappears is not the dominant frequency. The previous analysis method always used the dominant frequency of the fringe subset for signal analysis since it produced the best signal to noise ratio. The frequencies at which the SvB algorithm identified insensitivity to surface binding was never at the dominant frequency. The S/N value varied between the fringe-frequency subsets but the particular signals shown in Figure 9-c and d had S/N of 3.56 and 2.98, respectively. This translates to a 16% reduction in S/N for this case. The S/N varied with each unique

fringe-frequency subset found but the SvB algorithm analysis was inferior to the previous analysis method for all cases in this regard. Efforts were made to increase the S/N of the signal using the SvB algorithm method. There were many cases in which multiple frequencies within a single fringe subset exhibited the bulk signal and no surface signal. In these cases we found it possible to increase the S/N, while maintaining discrimination of the bulk signal, by simply summing these multiple fringe-frequency

start fringe	end fringe	frequency	S/N	S/N after summing	% S/N increase
1	57	29	2.72	3.57	31.25
1	57	30	3.28		8.84
0	46	28	3.34	3.82	14.37
0	46	34	2.80		36.43
1	53	27	2.79	4.10	46.95
1	53	28	3.36		22.02
1	53	30	3.40		20.59
1	49	25	2.40	3.82	59.17
1	49	26	3.31		15.41
1	49	28	3.47		10.09

Table 3- Increase in signal to noise ratio occurs when data from fringe-frequency subsets are summed. The summed data have the same fringe subset with different frequencies represented in each. The summed subsets are contained within bold borders. Corresponding increases in signal to noise ratios are given.

subsets. Table 3 shows the magnitude of signal to noise increase using this method for various subsets. The first and second column show the first and last fringes of the specific subsets being summed, respectively. The third column shows the different frequencies within the fringe subset. For example, the first two rows in Table 3 show two fringe-frequency subsets that were summed. Both subsets were between fringes 1 and 57 but had different frequencies of 29 and 30 cycles per window. The S/N was calculated for each subset and is shown in column 4. The S/N was calculated again after the signals from the two fringe-frequency subsets were summed and is shown in column 5. The last column in Table 3 shows the percentage increase in S/N after the summing was performed.

There are potential ways to utilize this algorithm to improve S/N ratios for assays whose S/N is decreased due to inconsistent surface adhesion between samples. For example, because MEPTES is now

known to alter the BSI signal when applied to the channel surface, a small section of the channel could be coated with MEPTES to provide calibration. Signal from a glycerol gradient in the bulk fluid of the channel could be obtained with and without the MEPTES present. The SvB algorithm would then be run to find the fringe-frequency subsets that eliminate the signal produced by the MEPTES and this subset could then be used to analyze the signal from samples of interest. In theory, because the fringe-frequency subset found by the SvB algorithm is not sensitive to what happens on the surface of the channel, the surface adhesion from the samples of interest would not affect the signal. In this way, the inconsistencies on the channel surface that degrade the S/N would be ignored and the S/N would increase.

Conclusions

We demonstrated a new fringe pattern interrogation method that has the potential to distinguish signals produced at the surface from those in the free-solution. Using a greater number of fringes and analyzing sub-frequencies, we found that the fringe pattern produced by BSI has multiple fringe-frequency subsets that report only changes in the bulk fluid but not at the channel surface. Using a less dominant frequency has the disadvantage of slightly degrading the S/N produced by BSI, but summing two or more of the these sub-frequencies improves performance so as to approach the conventional assay methodology. The algorithm is user friendly, allows predetermined parameters to be selected to set signal quality thresholds, outputs these subsets, and reports at which fringes, and at what frequency within those fringes, to perform analysis in order to eliminate signal being produced from the surface of the channel. Alternatively it is possible to select the frequencies of analysis so as to eliminate the bulk signal, as would be desirable for tethered assays. We are currently testing the SvB methodology for the ability to improve the reproducibility of measurements of challenging assays such as those performed in high percentages of serum, on tissue homogenates, or with samples that have significant non-specific binding to the channel.

Acknowledgment

This work was supported by the NSF (Grants CHE-0848788 and CHE-1307899) as well as the National Institute of Health and The Bill and Melinda Gates Foundation.

Appendix

A. Criteria Illustration

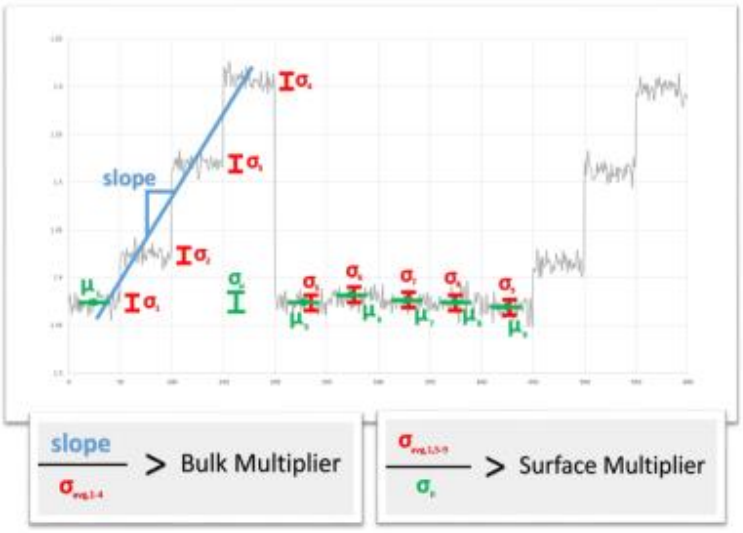

B. Program Flowchart

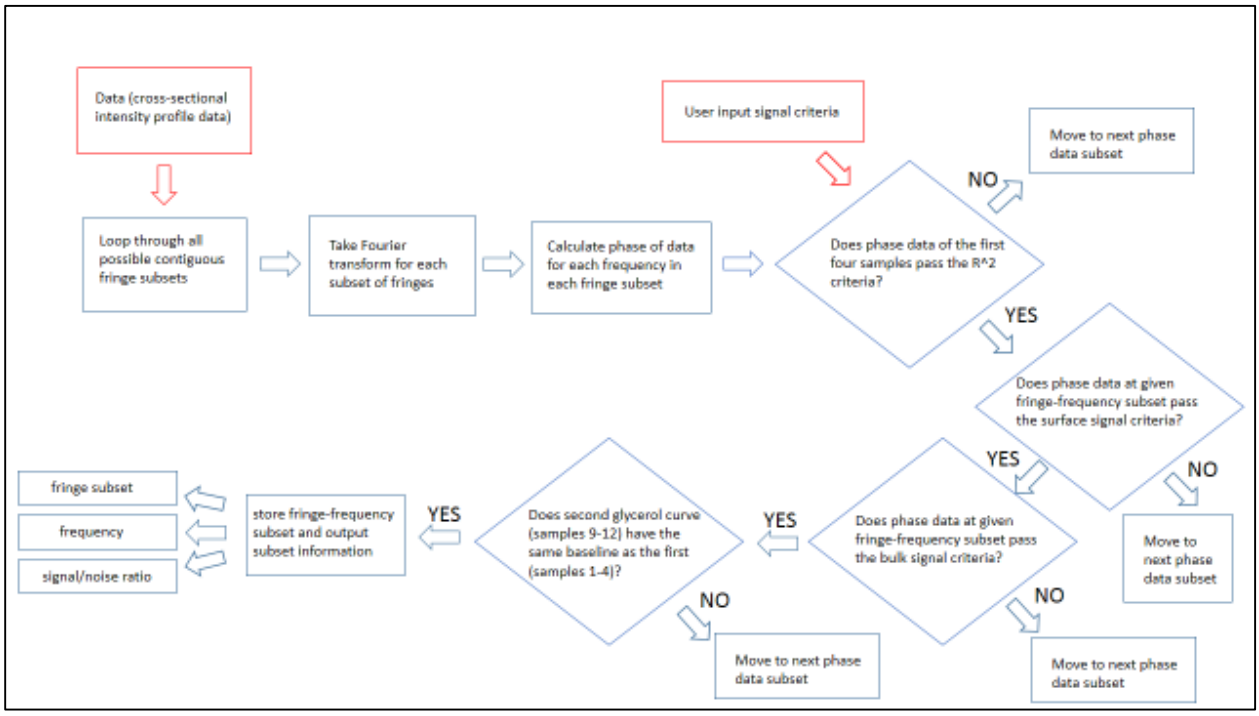

C. LabVIEW Code (version 2012 SP1 32-bit)

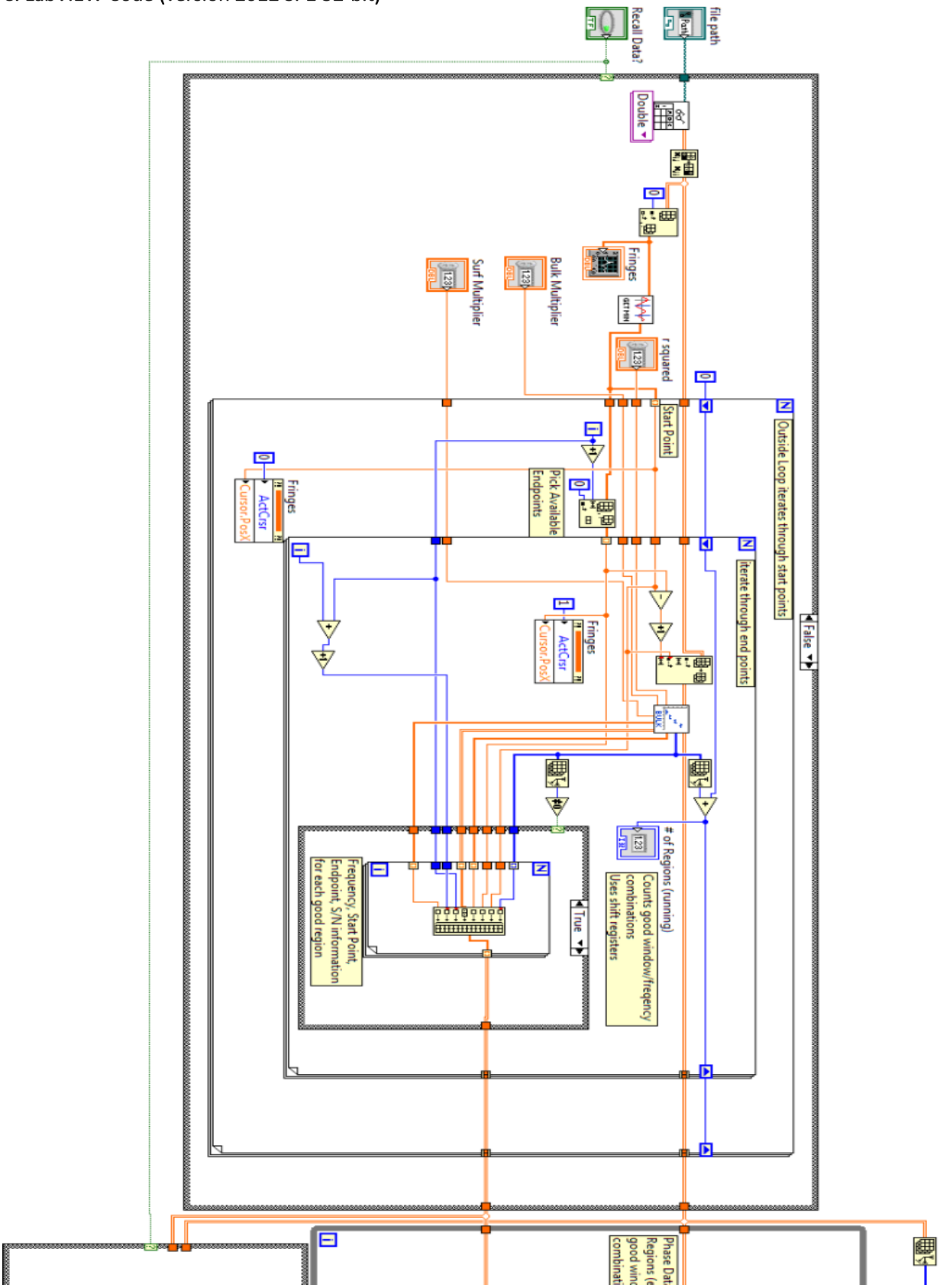

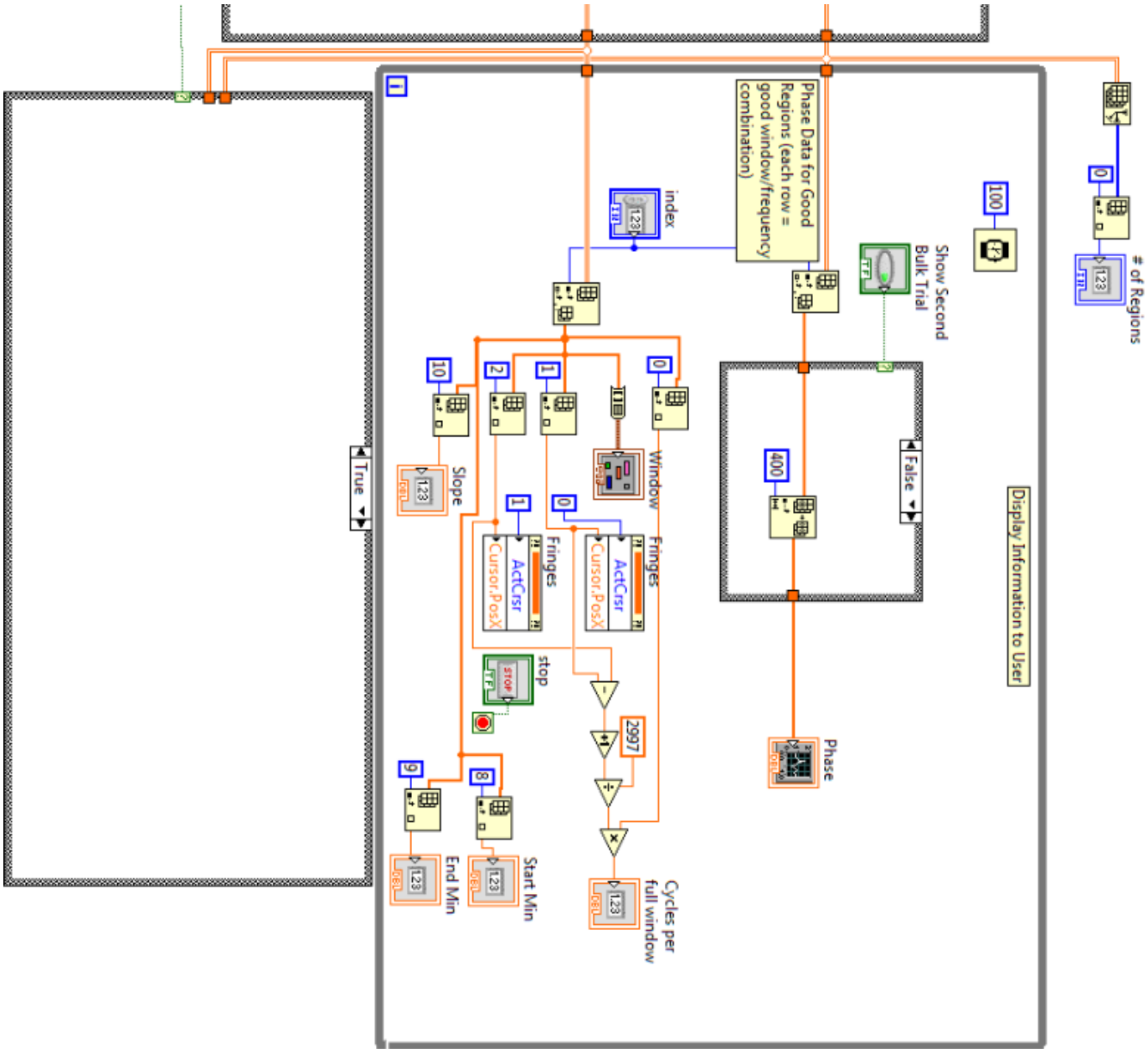
Display Information to User
Phase Data for Good Regions (each row = good window/frequency combination)
index
Show Second Bulk Trial
# of Regions
100
400
False
True
Phase
Window
Fringes
Cursor.PosX
ActCrsr
Slope
stop
2997
Cycles per full window
Start Min
End Min

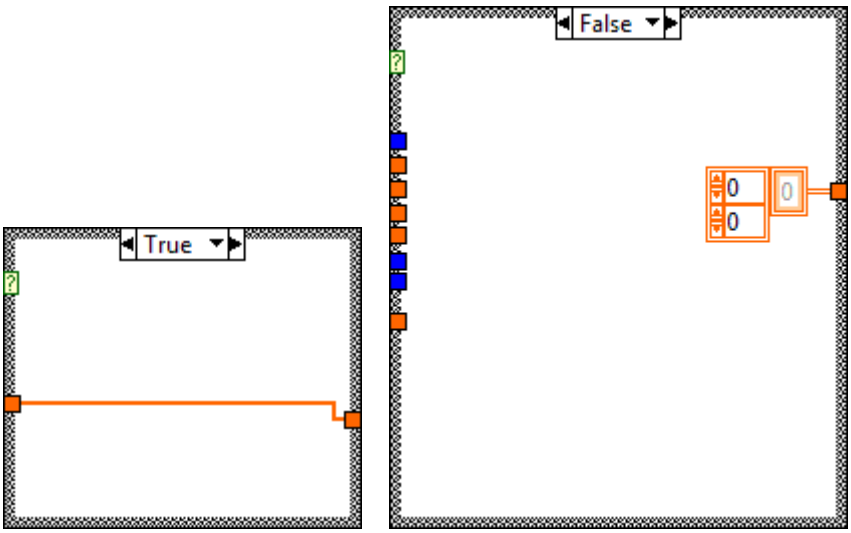
False
True
0
0
0

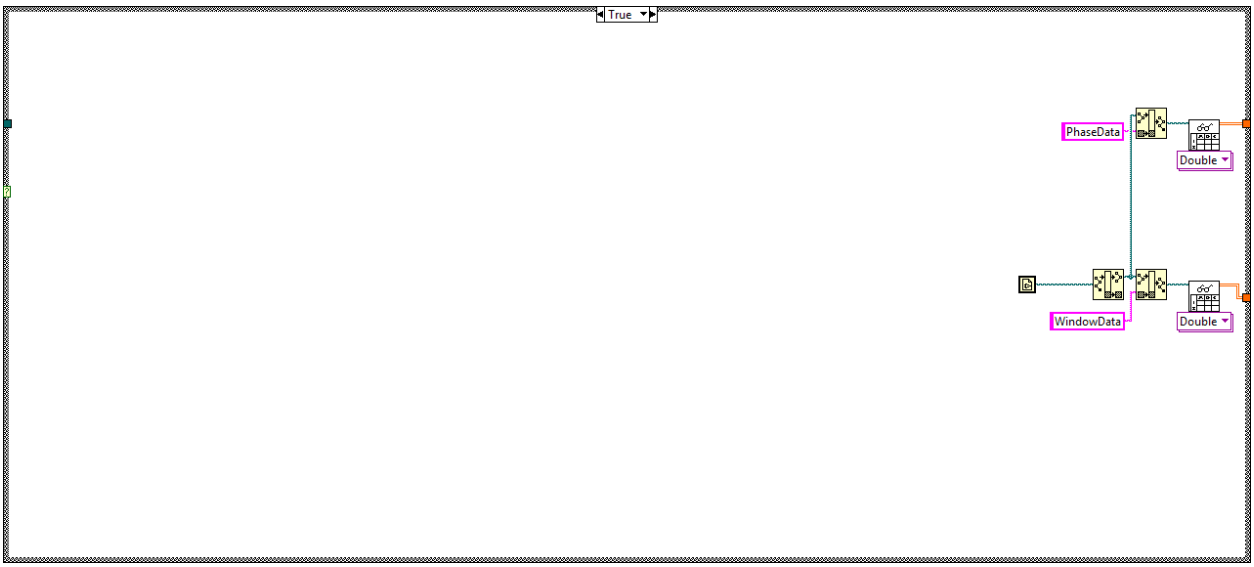
True
PhaseData
Double
WindowData
Double

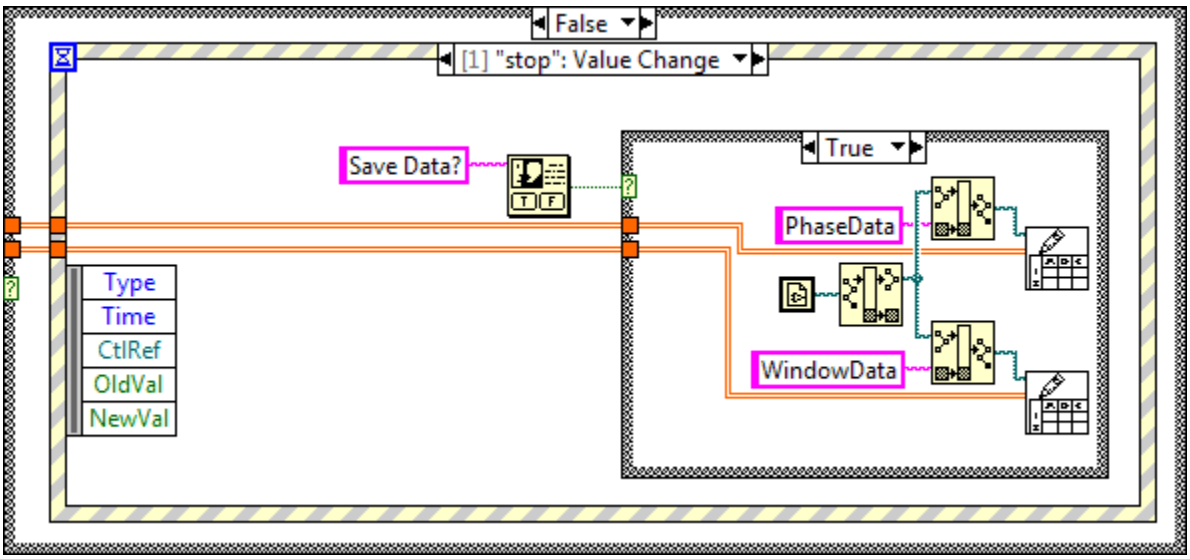
False
[1] "stop": Value Change
Save Data?
True
PhaseData
WindowData
Type
Time
CtlRef
OldVal
NewVal

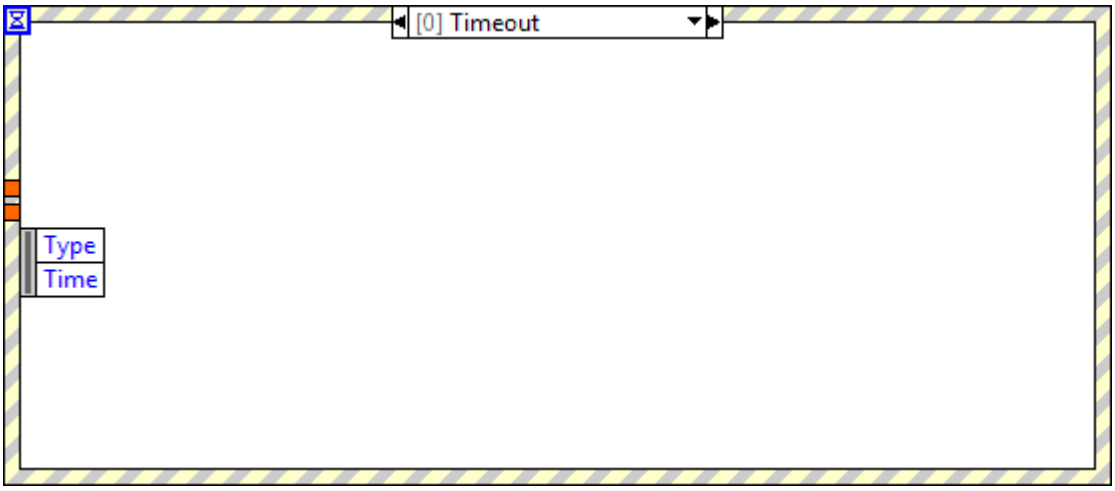
[0] Timeout
Type
Time

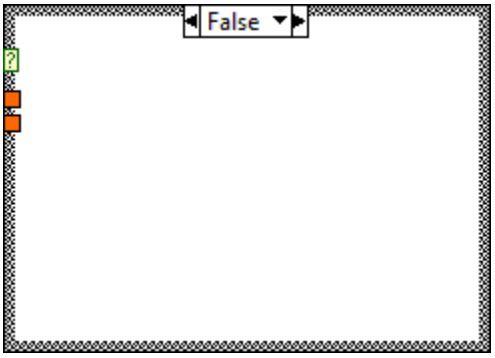
False

REFERENCES

1. Sabban, S., *Development of an in vitro model system for studying the interaction of Equus caballus IgE with its high-affinity FcεRI receptor*, 2011, University of Sheffield.
2. Kussrow, A., C.S. Enders, and D.J. Bornhop, *Interferometric methods for label-free molecular interaction studies.* Analytical Chemistry, 2011. **84**(2): p. 779-792.
3. Swann, M.J., et al., *Dual-polarization interferometry: an analytical technique to measure changes in protein structure in real time, to determine the stoichiometry of binding events, and to differentiate between specific and nonspecific interactions.* Analytical biochemistry, 2004. **329**(2): p. 190-198.
4. Brody, E.N., et al., *High-content affinity-based proteomics: unlocking protein biomarker discovery.* Expert review of molecular diagnostics, 2010. **10**(8): p. 1013-1022.
5. Boozer, C., et al., *Looking towards label-free biomolecular interaction analysis in a high-throughput format: a review of new surface plasmon resonance technologies.* Current Opinion in Biotechnology, 2006. **17**(4): p. 400-405.
6. Merchant, M., et al., *Monovalent antibody design and mechanism of action of onartuzumab, a MET antagonist with anti-tumor activity as a therapeutic agent.* Proceedings of the National Academy of Sciences, 2013. **110**(32): p. E2987-E2996.
7. Miller, S.C., et al., *Identification of known drugs that act as inhibitors of NF-κB signaling and their mechanism of action.* Biochemical pharmacology, 2010. **79**(9): p. 1272-1280.
8. Araujo, R.P., L.A. Liotta, and E.F. Petricoin, *Proteins, drug targets and the mechanisms they control: the simple truth about complex networks.* Nature Reviews Drug Discovery, 2007. **6**(11): p. 871-880.
9. Agoram, B.M., S.W. Martin, and P.H. van der Graaf, *The role of mechanism-based pharmacokinetic–pharmacodynamic (PK–PD) modelling in translational research of biologics.* Drug discovery today, 2007. **12**(23): p. 1018-1024.
10. Lowe, P.J., et al., *On Setting the First Dose in Man: Quantitating Biotherapeutic Drug-Target Binding through Pharmacokinetic and Pharmacodynamic Models.* Basic & clinical pharmacology & toxicology, 2010. **106**(3): p. 195-209.
11. Yu, L.J., et al., *Establishment of correlation between in vitro enzyme binding potency and in vivo pharmacological activity: application to liver glycogen phosphorylase a inhibitors.* The Journal of pharmacology and experimental therapeutics, 2006. **317**(3): p. 1230-1237.
12. Choo, S., et al., *Enzyme activity measurements using bio-layer interferometry*, 2008, Google Patents.
13. Kabashin, A. and P. Nikitin, *Interferometer based on a surface-plasmon resonance for sensor applications.* Quantum Electronics, 1997. **27**(7): p. 653-654.
14. Kabashin, A. and P. Nikitin, *Surface plasmon resonance interferometer for bio-and chemical-sensors.* Optics Communications, 1998. **150**(1): p. 5-8.
15. Homola, J., S.S. Yee, and G. Gauglitz, *Surface plasmon resonance sensors: review.* Sensors and Actuators B: Chemical, 1999. **54**(1): p. 3-15.
16. Fan, X., et al., *Sensitive optical biosensors for unlabeled targets: A review.* analytica chimica acta, 2008. **620**(1): p. 8-26.
17. Guo, J., P.D. Keathley, and J. Hastings, *Dual-mode surface-plasmon-resonance sensors using angular interrogation.* Optics letters, 2008. **33**(5): p. 512-514.
18. Cooper, M.A., *Label-free screening of bio-molecular interactions.* Analytical and bioanalytical chemistry, 2003. **377**(5): p. 834-842.

19. Ladbury, J.E., G. Klebe, and E. Freire, *Adding calorimetric data to decision making in lead discovery: a hot tip.* Nature Reviews Drug Discovery, 2010. **9**(1): p. 23-27.
20. Tu, X., et al., *Thermal independent silicon-nitride slot waveguide biosensor with high sensitivity.* Optics express, 2012. **20**(3): p. 2640-2648.
21. Passaro, V., et al., *Guided-wave optical biosensors.* Sensors, 2007. **7**(4): p. 508-536.
22. Brosinger, F., et al., *A label-free affinity sensor with compensation of unspecific protein interaction by a highly sensitive integrated optical Mach–Zehnder interferometer on silicon.* Sensors and Actuators B: Chemical, 1997. **44**(1): p. 350-355.
23. Prieto, F., et al., *An integrated optical interferometric nanodevice based on silicon technology for biosensor applications.* Nanotechnology, 2003. **14**(8): p. 907.
24. Ymeti, A., et al., *Realization of a multichannel integrated Young interferometer chemical sensor.* Applied optics, 2003. **42**(28): p. 5649-5660.
25. Hradetzky, D., C. Mueller, and H. Reinecke, *Interferometric label-free biomolecular detection system.* Journal of Optics A: Pure and Applied Optics, 2006. **8**(7): p. S360.
26. Schneider, B., et al., *Optical chip immunoassay for hCG in human whole blood.* Biosensors and Bioelectronics, 2000. **15**(11): p. 597-604.
27. Wang, J., et al., *Real-time study of genomic DNA structural changes upon interaction with small molecules using dual-polarization interferometry.* Analytical Chemistry, 2009. **81**(12): p. 4914-4921.
28. Wang, J., et al., *Optical Extinction Combined with Phase Measurements for Probing DNA− Small-Molecule Interactions Using an Evanescent Waveguide Biosensor.* Analytical Chemistry, 2010. **82**(13): p. 5455-5462.
29. Qavi, A.J., et al., *Label-free technologies for quantitative multiparameter biological analysis.* Analytical and bioanalytical chemistry, 2009. **394**(1): p. 121-135.
30. Luchansky, M.S., et al., *Sensitive on-chip detection of a protein biomarker in human serum and plasma over an extended dynamic range using silicon photonic microring resonators and sub-micron beads.* Lab on a Chip, 2011. **11**(12): p. 2042-2044.
31. Qavi, A.J., J.T. Kindt, and R.C. Bailey, *Sizing up the future of microRNA analysis.* Analytical and bioanalytical chemistry, 2010. **398**(6): p. 2535-2549.
32. Ouyang, H., et al., *Label-free quantitative detection of protein using macroporous silicon photonic bandgap biosensors.* Analytical Chemistry, 2007. **79**(4): p. 1502-1506.
33. Proll, G., et al., *Reflectometric interference spectroscopy*, in *Biosensors and Biodetection*2009, Springer. p. 167-178.
34. Gauglitz, G., *Direct optical sensors: principles and selected applications.* Analytical and bioanalytical chemistry, 2005. **381**(1): p. 141-155.
35. Lin, V.S.-Y., et al., *A porous silicon-based optical interferometric biosensor.* science, 1997. **278**(5339): p. 840-843.
36. Markov, D.A., K. Swinney, and D.J. Bornhop, *Label-free molecular interaction determinations with nanoscale interferometry.* Journal of the American Chemical Society, 2004. **126**(50): p. 16659-16664.
37. Latham, J.C., et al., *Photobiotin Surface Chemistry Improves Label-Free Interferometric Sensing of Biochemical Interactions.* Angewandte Chemie International Edition, 2006. **45**(6): p. 955-958.
38. Bornhop, D.J., et al., *Free-solution, label-free molecular interactions studied by back-scattering interferometry.* science, 2007. **317**(5845): p. 1732-1736.
39. Baksh, M.M., et al., *Label-free quantification of membrane-ligand interactions using backscattering interferometry.* Nature biotechnology, 2011. **29**(4): p. 357-360.
40. Xi, B., et al., *The application of cell-based label-free technology in drug discovery.* Biotechnology journal, 2008. **3**(4): p. 484-495.

41. Kussrow, A., et al., *Measurement of Monovalent and Polyvalent Carbohydrate− Lectin Binding by Back-Scattering Interferometry.* Analytical Chemistry, 2009. **81**(12): p. 4889-4897.
42. Olmsted, I.R., et al., *Measurement of aptamer–protein interactions with back-scattering interferometry.* Analytical Chemistry, 2011. **83**(23): p. 8867-8870.
43. Kussrow, A., et al., *The potential of backscattering interferometry as an in vitro clinical diagnostic tool for the serological diagnosis of infectious disease.* Analyst, 2010. **135**(7): p. 1535-1537.
44. Adams, N.M., et al., *The effect of hybridization-induced secondary structure alterations on RNA detection using backscattering interferometry.* Nucleic acids research, 2013. **41**(9): p. e103-e103.
45. Tiefenbrunn, T., et al., *Small molecule regulation of protein conformation by binding in the flap of HIV protease.* ACS chemical biology, 2013. **8**(6): p. 1223-1231.
46. Norde, W., *Adsorption of proteins from solution at the solid-liquid interface.* Advances in Colloid and Interface Science, 1986. **25**(0): p. 267-340.
47. Norde, W., et al., *Protein adsorption at solid-liquid interfaces: Reversibility and conformation aspects.* Journal of Colloid and Interface Science, 1986. **112**(2): p. 447-456.
48. Graham, D.E. and M.C. Phillips, *Proteins at liquid interfaces: I. Kinetics of adsorption and surface denaturation.* Journal of Colloid and Interface Science, 1979. **70**(3): p. 403-414.
49. Suelter, C. and M. DeLuca, *How to prevent losses of protein by adsorption to glass and plastic.* Analytical biochemistry, 1983. **135**(1): p. 112-119.
50. Pesciotta, E.N., D.J. Bornhop, and R.A. Flowers, *Back-Scattering Interferometry: A Versatile Platform for the Study of Free-Solution versus Surface-Immobilized Hybridization.* Chemistry-an Asian Journal, 2011. **6**(1): p. 70-73.
51. Sørensen, H.S., et al., *Highly sensitive biosensing based on interference from light scattering in capillary tubes.* Applied physics letters, 2006. **89**(15): p. 151108.
52. Golosovsky, M., et al., *Midinfrared surface-plasmon resonance: A novel biophysical tool for studying living cells.* Journal of applied physics, 2009. **105**(10): p. 102036.
53. Silin, V., H. Weetall, and D.J. Vanderah, *SPR studies of the nonspecific adsorption kinetics of human IgG and BSA on gold surfaces modified by self-assembled monolayers (SAMs).* Journal of Colloid and Interface Science, 1997. **185**(1): p. 94-103.
54. Uchida, K., et al., *A reactive poly (ethylene glycol) layer to achieve specific surface plasmon resonance sensing with a high S/N ratio: the substantial role of a short underbrushed PEG layer in minimizing nonspecific adsorption.* Analytical Chemistry, 2005. **77**(4): p. 1075-1080.
55. Markov, D., D. Begari, and D.J. Bornhop, *Breaking the 10-7 barrier for RI measurements in nanoliter volumes.* Analytical Chemistry, 2002. **74**(20): p. 5438-5441.
56. Olmsted, I.R., A. Kussrow, and D.J. Bornhop, *Comparison of Free-Solution and Surface-Immobilized Molecular Interactions Using a Single Platform.* Analytical Chemistry, 2012. **84**(24): p. 10817-10822.